# Modeling and design of two-dimensional membrane-type active acoustic metamaterials with tunable anisotropic density

Ahmed Allam*
*Group for Advanced Research in Dynamic Systems,*
*Mechatronics Department, Ain Shams University, Cairo, 11517, Egypt*

Adel Elsabbagh and Wael Akl
*Group for Advanced Research in Dynamic Systems,*
*Design and Production Engineering Department, Ain Shams University, Cairo, 11517, Egypt*
(Dated: October 18, 2016)

A two-dimensional active acoustic metamaterial with controllable anisotropic density is introduced. The material consists of composite lead-lead zirconate titanate plates clamped to an aluminum structure with air as the background fluid. The effective anisotropic density of the material is controlled, independently for two orthogonal directions, by means of an external static electric voltage signal. The material is used in the construction of a reconfigurable waveguide capable of controlling the direction of the acoustic waves propagating through it. An analytic model based on the acoustic two-port theory, the theory of piezoelectricity, the laminated pre-stressed plate theory and the S-parameters retrieval method is developed to predict the behavior of the material. The results are verified using the finite element method. Excellent agreement is found between both models for the studied frequency and voltage ranges. The results show that, below 1600 Hz, the density is controllable within orders of magnitude relative to the uncontrolled case. The results also suggest that simple controllers could be used to program the material density towards full control of the directivity and dispersion characteristics of acoustic waves.

PACS numbers: PACS: 40.Dx, 40.Fz, 50.Gf

## I. INTRODUCTION

Acoustic metamaterials (AMM) are artificial materials with engineered sub-wavelength structures that possess acoustic material properties which are not readily available in nature including negative mass density [1, 2], negative bulk modulus [3, 4], double negative properties [5, 6] and large anisotropic properties [7–9]. With the aid of transformation acoustics techniques, these anomalous properties could be spatially distributed to construct devices which were otherwise difficult to fabricate; examples of such devices include acoustic superlens [10], acoustic cloaking [11–13] and nearly perfect sound absorbers [14]. AMM have been realized using different approaches. For instance, they were constructed by the use of sub-wavelength sonic crystals consisting of cylindrical scatterers in a background fluid [15]. Another approach is based on the use of sub-wavelength local resonators embedded in a background fluid. This was demonstrated by several techniques including the use of mass-in-mass AMM in which the unit cell of the material consists of a solid core material with relatively high density and a coating of elastically soft material [16], an array of elastic membranes placed transversely in a wave guide [2, 17, 18], arrays of Helmholtz resonators flush mounted to the walls of a wave guide [6, 19], as well as AMM with both elastic membranes and Helmholtz resonators/side branches [20, 21]. Another approach incorporates the use of elastic plates with local resonators in the form of mass spring resonators [22], or resonating composite stubs [23, 24].
The nature of AMM allows for controlling their material properties by integrating active elements inside their structure. Active piezoelectric patches were used to control the band gaps present in the material[25–29], construct tunable elastic waveguides[30, 31] and even control the directivity of elastic waves[27, 32].
Membrane type Acoustic Metamaterials (MAM) have a relatively simple cell structure which facilitates their characterization and implementation; nevertheless, they operate in a limited frequency range; moreover, because of their resonant nature, they are very sensitive to geometrical variations in the membrane structure and boundary conditions. To overcome these limitations, as well as provide a mean to control the effective properties of the material, active elements have recently been used in MAM in order to construct active membrane-type acoustic metamaterials (AMAM). These elements are used to control the material properties of AMAM, and to enhance the frequency range of the desired material properties. This has been first demonstrated by Akl and Baz [33–35], where they used acoustic cavities with walls made of piezoelectric diaphragms. By controlling the stiffness of the diaphragms they were able to control the effective density of the material. Their cell design however was based on water as a background material in the cavity, in addition to the need of a complex feedback control system. Chen et al. [36] suggested the use of gradient magnetic fields to actively tune the material properties of MAM. They suggested an AMAM cell made

* a.allam@eng.asu.edu.eg; Corresponding author.

of an aluminum circular ring with a magnetorheological elastomer at the center. They used a magnetic field to control the stiffness of the elastomer and hence the effective density. Their approach however was limited to tuning the effective properties of the cell near the first mode of the membrane. Xiao et al. [37] suggested the use of an electric field formed between a fishnet electrode and a metal coated central platelet attached to a circular rubber membrane. Their design required the application of voltages exceeding 300 $V$ to control the effective density within a limited frequency range.

Aiming for a simpler and hence more practical approach, we propose a novel design for AMAM consisting of composite lead-PZT plates supported on an aluminum frame with air as a background fluid. The stiffness of the plate is controlled by the application of an electric potential difference across the PZT layers; this enables us to control the effective (homogenized) density of the AMAM within a wide range of values ranging from negative to positive density values passing by near zero conditions. This is done with a limited effect on the effective bulk modulus and thus directly controlling the effective speed of sound in the material. This kind of control would open the door for the realization of various devices whose operation depends on the spatial distribution of density between positive and negative values, as well as density near zero (DNZ) applications.

This work is divided into six sections. In the first section a brief introduction is presented. In the 'Theoretical formulation' section, the construction of the suggested metamaterial cell is introduced, and a retrieval approach for the characterization of passive AMM is extended to be applied for active AMM. In the 'Numerical model' section, a numerical model is constructed to verify the analytic model using the finite element method (FEM). In the 'Results and discussion' section, the results obtained from both models are compared, and the overall performance of the new design is evaluated and analyzed. In the 'Applications' section the developed material is used the design of a programmable waveguide. Finally, a brief summary of the conclusion and outlines of the future work are presented.

## II. THEORETICAL FORMULATION

The suggested design for a practical 2D AMAM cell (Fig. 1) is inspired from the structure of the passive MAM developed by Gu et al.[38]. The main building block of the structure (Fig. 1d) consists of a composite lead-PZT circular plate clamped to a relatively thick (rigid) aluminum structure, and suspended in air. The composite plate has a diameter of 22 $mm$, and consists of three different layers. The middle layer is made of a lead alloy of thickness 50 $\mu m$, and extends through the diameter of the plate. Two piezoelectric layers made of PZT-5A material are deposited on the two sides of the middle layer, each of thickness 125 $\mu m$. The two layers have a shape of an annulus with inner diameter of 14 $mm$ and the same outer diameter as the plate. They are both polled in the thickness direction, and both have the same polling direction. The composite plate is fixed to a square aluminum frame of thickness 1 $mm$. The dimensions of the AMAM cell and the material properties of the different components are summarized in Table I and Table II respectively.

TABLE I. Summary of the dimensions of the AMAM cell.

| Dimension | Unit | Value |
|---|---|---|
| Cell constant ($a$) | $mm$ | 23 |
| Outer radius of the composite plate ($R_2$) | $mm$ | 11 |
| Inner radius of the composite plate ($R_1$) | $mm$ | 7 |
| Thickness of the lead layer ($t_1$) | $\mu m$ | 20 |
| Thickness of the piezoelectric layer ($t_2$) | $\mu m$ | 125 |
| Thickness of the aluminum frame ($t_3$) | $mm$ | 1 |

TABLE II. Properties of the materials used in the construction of the AMAM cell.

| Property | Unit | PZT-5A | Lead | aluminum |
|---|---|---|---|---|
| $\rho$ | $kg/m^3$ | 7500 | 11000 | 2700 |
| $C_{11}$ | $GPa$ | 132 | 75.9 | 102 |
| $C_{12}, C_{23}$ | $GPa$ | 73 | 62 | 50 |
| $C_{33}$ | $GPa$ | 115 | 75.9 | 102 |
| $e_{31}$ | $C/m^2$ | $-4.1$ | - | - |
| $e_{33}$ | $C/m^2$ | 14.3 | - | - |
| $\epsilon_{11}$ | | 804.6 | - | - |
| $\epsilon_{33}$ | | 659.7 | - | - |
| $Q_m = \eta^{-1}$ | | 50 | 50 | - |

The material properties of the cell are controlled by applying a static electric voltage across the thickness of two annular piezoelectric layers as shown in Fig. 1d. The applied electric voltage induces stresses in the piezoelectric layers which changes the tension applied on the middle circular lead membrane. This in turn changes the acoustic impedance, and hence the effective material properties of the cell.

A controllable DC voltage source is connected between the outer surfaces of the piezoelectric layers, which are connected in series. Both are polled in the same direction; thus, any bending of the composite plate due to incident acoustic waves will cause the stretching of one layer and the compression of the other. This will cause equal but opposite voltages to be generated by the two layers, and due to the series connection almost no time dependent current will be generated. Thus, for all the subsequent analysis open circuit boundary conditions will be assumed for any dynamic analysis of the plate.

The 2D material is constructed by repeating the 1D unit cell (Fig. 1d) in two orthogonal directions to form the 2D unit cell shown in Fig. 1b. The cell constant $a$ is assumed to be much smaller than the wavelength of the incident

acoustic wave, thus homogenized effective material properties could be used to describe the wave propagation in the material. One of the methods for estimating these homogenized properties is the acoustic two-port theory, which is introduced briefly in the following section.

### A. Acoustic two-port theory

The acoustic two-port theory, also known as 'Acoustic transmission line theory', is commonly used to analyze acoustic duct networks at low frequencies [39]. It has recently been used to characterize AMM for different configurations [20, 40, 41]. One of the main elements of the acoustic two port theory is the transfer matrix which relates the acoustic pressure ($p$) and volume velocity ($v$) at point $a$ to the pressure and volume velocity at point $b$ through the relation:

$$\begin{bmatrix} p_a \\ v_a \end{bmatrix} = \boldsymbol{T} \begin{bmatrix} p_b \\ v_b \end{bmatrix}, \boldsymbol{T} = \begin{bmatrix} T_{11} & T_{12} \\ T_{21} & T_{22} \end{bmatrix} \tag{1}$$

Equation (1) is useful when connecting two networks in series, as it is the case in layered AMM. Given a metamaterial cell consisting of $n$ cascaded layers with different material properties, the transfer matrix of the whole cell can be written as:

$$\boldsymbol{T}_{cell} = \boldsymbol{T}_1 \boldsymbol{T}_2 \ldots \boldsymbol{T}_n \tag{2}$$

Where $\boldsymbol{T}_1, \boldsymbol{T}_2, \ldots, \boldsymbol{T}_n$ are the transfer matrices of each layer. For an acoustic layer with acoustic impedance $Z_n$ and thickness $t_n$, the transfer matrix can be calculated from the relation [39]:

$$\boldsymbol{T}_n = \begin{bmatrix} \cos(k_n t_n) & jZ_n \sin(k_n t_n) \\ j\sin(k_n t_n)/Z_n & \cos(k_n t_n) \end{bmatrix} \tag{3}$$

Where $k_n = \omega / c_n$ is the wave number of the acoustic wave in layer $n$, $\omega$ is the angular frequency of the incident acoustic wave, $c_n$ is the speed of sound in the layer and $j = \sqrt{-1}$ is the engineering complex number. Another important element of the acoustic two port theory is the scattering matrix which relates the incident and scattered wave pressures on an acoustic sample (Fig. 2). The scattering matrix formulation is given by:

$$\begin{bmatrix} p_a^- \\ p_b^+ \end{bmatrix} = \boldsymbol{S} \begin{bmatrix} p_a^+ \\ p_b^- \end{bmatrix}, \boldsymbol{S} = \begin{bmatrix} S_{11} & S_{12} \\ S_{21} & S_{22} \end{bmatrix} \tag{4}$$

Where $p_a^{\pm}, p_b^{\pm}$ are the complex pressures traveling in the positive and negative directions at points $a$ and $b$ respectively. The scattering matrix can be calculated from the elements of the transfer matrix from[42]:

$$\boldsymbol{S} = \begin{bmatrix} 1 & -T_{11} - \frac{T_{12}}{Z_b} \\ -\frac{1}{Z_a} & -T_{21} - \frac{T_{22}}{Z_b} \end{bmatrix}^{-1} \begin{bmatrix} -1 & T_{11} - \frac{T_{12}}{Z_b} \\ -\frac{1}{Z_a} & T_{21} - \frac{T_{22}}{Z_b} \end{bmatrix} \tag{5}$$

Where $Z_a$ and $Z_b$ are the acoustic impedance at points $a$ and $b$. The elements of the scattering matrix represent the complex pressure reflection and transmission coefficients ($R$, $T$) for incident upstream and downstream acoustic waves. For geometrically symmetric AMM cells the scattering matrix can be written as:

$$\boldsymbol{S} = \begin{bmatrix} R & T \\ T & R \end{bmatrix} \tag{6}$$

### B. Retrieval of the effective material properties

The effective material properties of AMM can be estimated by computing the elements of the transfer matrix or the scattering matrix of the material either analytically from the constitutive layers of the cell, experimentally or numerically. These elements are then compared to those of a homogeneous acoustic layer and the material properties are evaluated. Given that the elements of the transfer matrix for an AMM sample are determined, the effective material properties can be estimated using equation (3). For example, assuming that the effective parameters are $Z_{eff}, n_{eff}, t_{eff}$, they can be determined using:

$$n_{eff} = \frac{\pm cos^{-1}(T_{11}) + 2\pi m}{k_o t_{eff}}, Z_{eff} = \frac{-jT_{12}}{sin(n_{eff} k_o t_{eff})} \tag{7}$$

Where $n_{eff} = \frac{c_o}{c_{eff}} = \frac{k_{eff}}{k_o}$ is the effective refractive index of the material, $c_o, c_{eff}$ are the speed of sound in air and the effective speed of sound in the material respectively, $k_o$ is the acoustic wave number of the incident wave in air, $m = 0, 1, 2, \ldots$ . An equivalent approach employs the use of the Scattering matrix elements (S-parameters). This approach was first introduced in the electromagnetic domain [43–45] and later adapted to the acoustic domain [46]. It was used to calculate the effective constitutive material properties of an AMM from measuring the S-parameters from a sample consisting of a few number of cells down to a sample consisting of a single symmetric metamaterial cell [9, 40, 47, 48].
Using the S-parameters ($R$,$T$) instead of the transfer matrix elements the effective parameters $Z_{eff}, n_{eff}$ can be calculated by [46]:

$$n_{eff} = \frac{-j\ln(\phi) + 2\pi m}{k_o d}, Z_{eff} = \frac{\rho_o c_o q}{1 - 2R + R^2 - T^2} \tag{8}$$

Where

$$q = \pm\sqrt{(R^2 - T^2 - 1)^2 - 4T^2}, \phi = \frac{1 - R^2 + T^2 + q}{2T} \tag{9}$$

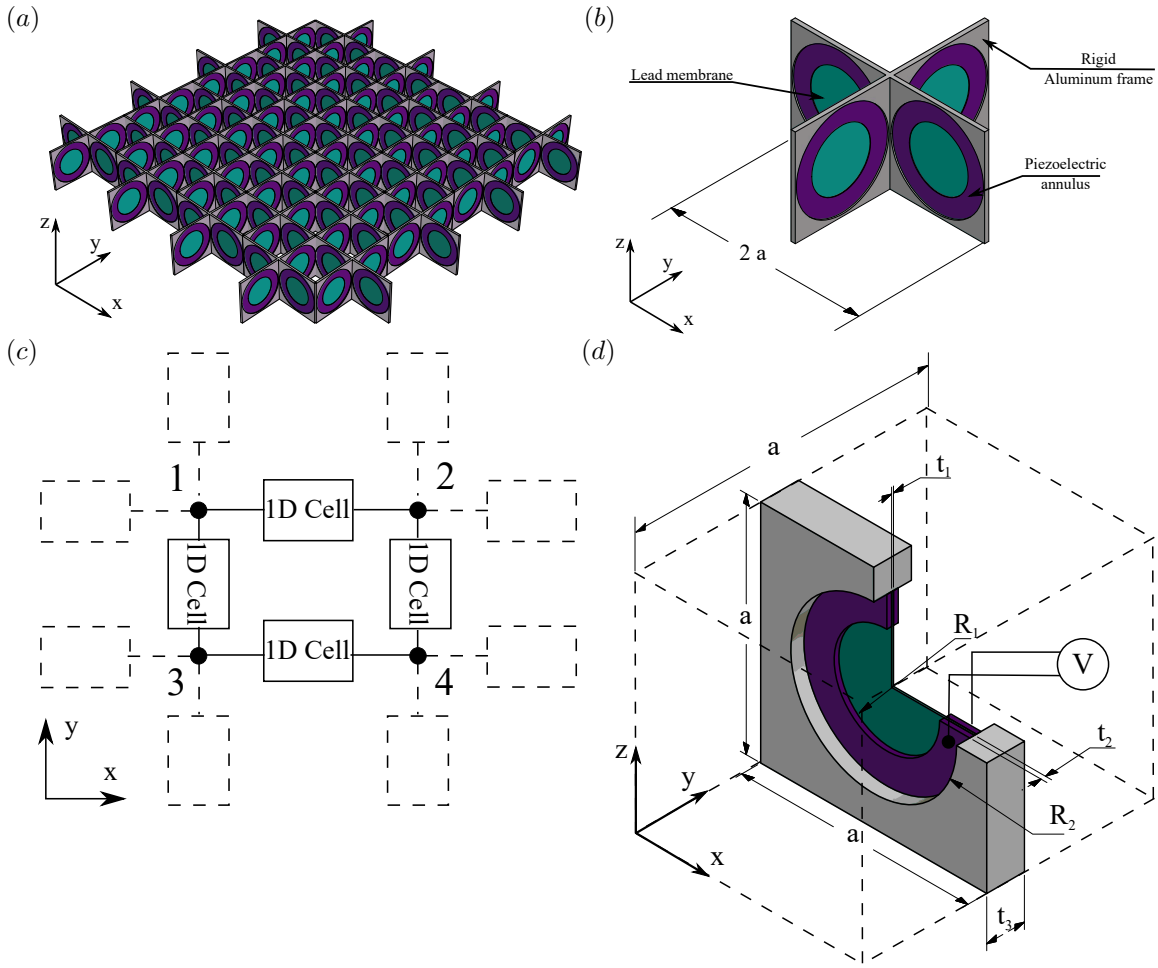


FIG. 1. A new concept for a 2D active membrane-type metamaterial. (a) A visualization for the construction of the suggested 2D AMAM. (b) Schematic representation for the 2D building block of the material. (c) Acoustic 2-Port representation for the building block. (d) Schematic representation of the construction of the 1D building block (1D AMAM cell).

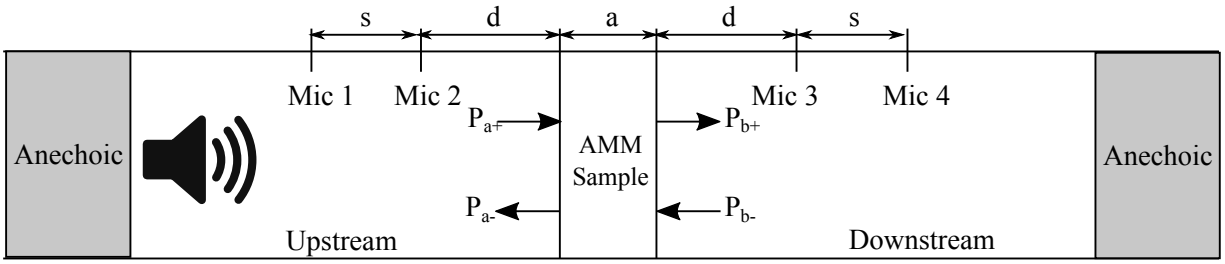


FIG. 2. Four microphone setup for estimating the scattering matrix of an acoustic sample.

$Z_{eff}, n_{eff}$ are related to the effective density and the effective bulk modulus of the AMM ($\rho_{eff}, B_{eff}$) by:

$$Z_{eff} = \rho_{eff} c_{eff}, n_{eff}^2 = \frac{\rho_{eff} c_o^2}{B_{eff}} \tag{10}$$

Reordering the equations, the effective properties can thus be calculated from

$$\rho_{eff} = \frac{n_{eff} Z_{eff}}{c_o}, B_{eff} = \frac{Z_{eff} c_o}{n_{eff}} \tag{11}$$

Two issues must be addressed before equations (7) to (11) can be used to uniquely determine the effective material properties of the AMM. The First is the estimation of the sign of $n_{eff}$. For passive AMM this issue is addressed by

imposing the real part of the acoustic impedance to be positive $Real(Z) \geq 0$, or the imaginary component of the refractive index to be negative $Imag(n_{eff}) \leq 0$. These constraints are generally not applicable to active AMM; nevertheless, assuming that the input energy to the cell is very small compared to the incident acoustic energy, these conditions should still be applicable. For the suggested cell, the applied voltage is considered to be static and thus virtually no energy is supplied to the cell. The second issue is the branching problem, which concerns the correct estimation of the branch number $m$. Fokin et al. [46] suggested determining the effective parameters of a minimum thickness AMM cell, for which $m$ is zero, and using this solution to estimate higher frequencies. Zhu et al. [40] suggested using an iterative approach to ensure the continuity of the parameters. On the other hand, Szabo et al. [45] suggested a more rigorous approach to estimate the branch number. They suggested an algorithm based on Kramers-Kronig relationship between the imaginary and real components of $n$ which uniquely determines the value of $m$. While their algorithm was only developed for electromagnetic metamaterials it has been reported to be used in acoustics [49]. And since it depends on fundamental physical relations based on the principle of causality [50], it can be used directly for the acoustic domain.

### C. Characterizing the 2D AMAM cell

One approach to analyze the proposed 2D structure of the AMAM cell, shown in Fig. 1b, is to consider it as four interconnected 1D AMAM cells. This is similar to what Gu et al.[38] have done for passive MAM using a lumped parameter model. Assuming that the transfer matrix (scattering matrix) for the 1D cell is known, the 2D cell could be modeled using the 2-Port network shown in Fig. 1c. In order to analyze this network, or networks formed by multiple cells, the formalism developed by Glav and Abom[51] for analyzing two-port networks will be used. Once the transfer matrix of each element in the cell is known, the formalism could be used to estimate the equivalent transfer matrix between any two nodes in the network. For example, in order to determine the effective properties of the material represented by Fig. 1c using only one cell, the formalism could be used to estimate the transfer matrix between nodes 1 and 2, for the properties in x-direction, and between 1 and 3 for the properties in y-direction. This could be easily extended to networks consisting of multiple cells.

### D. Characterizing the 1D AMAM cell

Since the 2D cell is modeled in terms of a network of 1D cells, the focus is on estimating the transfer matrix of the 1D cell. For waves propagating in the x-direction, the suggested cell, shown in Fig. 1d, consists of three main layers which are the elastic composite plate and two straight air layers. The local transfer matrix of every layer is calculated depending on the nature of the layer. The transfer matrix of the whole 1D metamaterial cell is then estimated using equation (2) and converted to the scattering matrix form.

The transfer matrices of the straight air layers can be easily determined from equation (3). In order to determine the transfer matrix of the third layer which is the elastic plate, the thickness of the composite plate is assumed to be small enough compared to the width of the cell ($a$) and the incident wavelength; thus, it could be assumed as a lumped element with lumped impedance ($Z$). For a lumped element the transfer matrix is given by [39]:

$$T = \begin{bmatrix} 1 & Z \\ 0 & 1 \end{bmatrix} \tag{12}$$

Where the acoustic impedance of a lumped element ($Z$) can be calculated from:

$$Z = \frac{p}{v} \tag{13}$$

Since the traverse velocity of the elastic plate is not uniform across its area, the averaged volume velocity over the area of the plate ($\widetilde{v}$) will be used to estimate its acoustic impedance. $\widetilde{v}$ is given by:

$$\widetilde{v} = \frac{1}{A_{cell}} \left( \frac{1}{A_{cell}} \int_{A_{cell}} \dot{w} dA \right) \tag{14}$$

Where $A_{cell}$ is the surface area of the square cell and $\dot{w}$ is the average point velocity of the plate.

The acoustic impedance of passive clamped elastic plates is a classical problem in acoustics [52], however we shall consider the active case where the plate is subjected to stresses caused by the piezoelectric effect. The lead membrane with the piezoelectric annulus will be treated as a composite circular plate consisting of two regions. The first region is the circular lead membrane with radius $R_1$, and the second is the outer annular region with inner radius $R_1$ and outer radius $R_2$. The annular region consists of multiple layers of different materials. The middle layer is the lead membrane which acts also as a metallic electrode for the lower and upper piezoelectric PZT layers. The other surfaces of the piezoelectric layers are coated with thin metallic electrodes. A static voltage $V$ is applied between the two metallic electrodes which induces in plane stresses in the composite plate. According to the classical composite thin plate theory, the equations of motion for the traverse deflection of an axisymmetric transversely isotropic composite plate can be written as

[53]:

$$
\begin{aligned}
&I_o \frac{\partial^2 w(r,t)}{\partial t^2} + D_{11}\nabla^4 w(r,t) - N\nabla^2 w(r,t) = p(r,t) \\
&I_o = \int_0^h \rho dz, \\
&D_{ij} = \int_0^h Q_{ij} z^2 dz, \\
&Q_{ij} = C_{ij} - \frac{C_{i3}C_{3j}}{C_{33}}
\end{aligned} \tag{15}
$$

Where $w(r,t)$ is the transverse deflection of the plate, $r$ is the radial distance from the center of the plate, $N$ is the in-plane force per unit tangent length, $p(r,t)$ is the pressure difference between the two sides of the plate, $\rho$ is the mass density of the different layers, $h$ is the total thickness of the plate and $C_{ij}$ are the elements of the stiffness matrix of the different layers of the plate. For the piezoelectric layers, since open circuit electrical boundary conditions are maintained, the stiffness matrix under constant electric displacement $\boldsymbol{C}^D$ will be used. Material damping is included in the analysis in the form of a complex stiffness matrix $\boldsymbol{C}^{D*}$.

$$
\boldsymbol{C}^{D*} = \boldsymbol{C}^D(1+\eta j) \tag{16}
$$

Where $\eta$ is loss factor inside the material. For harmonic excitation the incident acoustic pressure and the deflection of the plate could be written as:

$$
\begin{aligned}
p(r,t) &= P(r)e^{j\omega t}, \\
w(r,t) &= W(r)e^{j\omega t}
\end{aligned} \tag{17}
$$

Substituting in equation (15), canceling the exponentials and reordering:

$$
(\nabla^4 - \frac{N}{D_{11}}\nabla^2 - g^4)W(r) = \frac{P(r)}{D_{11}} \tag{18}
$$

Where $g$ is the complex wave number of the flexural waves traveling through the plate:

$$
g^4 = \frac{I_o\omega^2}{D_{11}} \tag{19}
$$

The solution of equation (18) can be written as the sum of the solution of the homogeneous equation and the solution of the particular equation. Since $\nabla$ is a linear operator, the homogeneous part of equation (18) can be written in the form:

$$
(\nabla^2 - g_1^2)(\nabla^2 + g_2^2)W(r) = 0 \tag{20}
$$

Where:

$$
g_1^2 = \frac{N + \sqrt{4D_{11}^2 g^4 + N}}{2D_{11}} \tag{21}
$$

$$
g_2^2 = \frac{-N + \sqrt{4D_{11}^2 g^4 + N}}{2D_{11}} \tag{22}
$$

For a polar coordinate system whose origin is at the center of the circular plate the complete solution of equation (18) is then:

$$
\begin{aligned}
W(r) =& E_1 J_0(g_1 r) + E_2 Y_0(g_1 r) \\
&+ E_3 I_0(g_2 r) + E_4 K_0(g_2 r) - \frac{P}{D_{11}g^4}
\end{aligned} \tag{23}
$$

Where $J_0(), I_0(), Y_0(), K_0()$ are the zeroth order Bessel and modified Bessel functions of the first and second kind. $E_1$ to $E_4$ are constants to be determined from the boundary and continuity conditions for each region of the plate.

In order to calculate the acoustic impedance of the plate it is required to calculate its area averaged displacement $\widetilde{W}$ which is given by:

$$
\widetilde{W} = \frac{1}{A_{cell}}\left(\int_0^{R_2} 2\pi r W(r) dr\right) \tag{24}
$$

The averaged volume velocity of the composite plate $\widetilde{v}$ is then given by:

$$
\widetilde{v} = \frac{j\omega\widetilde{W}}{A_{cell}} \tag{25}
$$

The acoustic impedance of the elastic layer $Z_e$ can then be calculated from the relation:

$$
Z_e = \frac{P}{\widetilde{v}} \tag{26}
$$

Only one issue remains before equation (26) can be used to determine the acoustic impedance of the composite plate, which is the estimation of the static in-plane forces $N_a, N_b$. This can be done by solving the static equation of motion for the in-plane displacements of the composite plate. It is given for axisymmetric displacements of a transversely isotropic plate by [53]

$$
\frac{\partial^2 u(r)}{\partial r^2} + \frac{1}{r}\frac{\partial u(r)}{\partial r} - \frac{u(r)}{r^2} = 0 \tag{27}
$$

The exact solution for equation (27) is given by:

$$
u(r) = E_5 r + \frac{E_6}{r} \tag{28}
$$

Where $E_5$ and $E_6$ are again constants to be determined from the boundary and continuity conditions for each region of the plate. The in-plane force $N$ is given as a

function of the in-plane displacement by:

$$N(r) = A_{11}u'(r) + \frac{A_{12}u(r)}{r} - N_p$$
$$A_{ij} = \int_0^h Q_{ij}dz \tag{29}$$

Where $N_p$ is the in-plane force due to the piezoelectric effect

$$N_p = \int_0^h \bar{e}_{31}^k E_3^k dz \tag{30}$$

$\bar{e}_{31}^k$ is the modified piezoelectric stress coefficient for layer $k$ and it is given by:

$$\bar{e}_{31}^k = e_{31}^k - \frac{C_{13}^k e_{33}^k}{C_{33}^k} \tag{31}$$

$E_3^k$ is the electric field across the thickness of layer $k$ and it is related to the applied voltage $V^k$ and the thickness of the layer $t^k$ by:

$$E_3^k = \frac{V^k}{t^k} \tag{32}$$

## III. NUMERICAL MODEL

In order to validate the analytic approach a 3D Piezo-Acoustic Finite Element Model (FEM) is developed using ANSYS commercial software. The model is constructed to mimic the 4-Microphone experimental procedure for the evaluation of the normal incidence sound transmission [54, 55]. The sample, whose material properties are to be determined, is placed in a rectangular impedance tube having the same cross-sectional area (Fig. 2). It is excited twice using a surface acoustic velocity source located once at the upstream end of the tube, and the other at the downstream end. Its response is captured by four virtual microphones located at the positions shown in Fig. 2. The distances $s, d$ were chosen as per the guidelines defined by the ASTM E2611[55]. The readings of the four microphones are then recorded and used to determine the S-matrix of the sample using the procedure found in [54].

The impedance tube is modeled as two acoustic domains (Upstream and Downstream), each domain is discretized using 20-node brick acoustic elements (FLUID220), and the length of each domain is 500 $mm$ long. The piezoelectric layers were discretized using 20-node brick coupled-field structural elements (SOLID226). The lead layer was discretized using 20-node brick structural elements (SOLID186). Since the aluminum structure is very rigid compared to the composite plate, it was modeled as rigid wall boundary conditions for the acoustic domain and fixed boundary conditions for the outer diameter of the composite plate. An infinite surface boundary condition was applied at the terminations of the impedance tube to model the anechoic terminations suggested by the 4-Microphone procedure. For each surface of the piezoelectric layers, the voltage degrees of freedom of the nodes forming it were coupled to simulate the effect of the presence of the thin metallic electrodes.

The solution is done in two steps; the stresses on the piezoelectric plates due to the applied voltage are determined using a static structural solution. The stresses calculated in the first step are then applied as pre-stresses on the composite plate in a linear perturbation harmonic analysis with incident acoustic pressure waves [56]. The harmonic analysis was carried at frequencies ranging between 400 $Hz$ and 1600 $Hz$ with a frequency step of 20 $Hz$. The element size of the piezoelectric/structural domain was chosen so that the error is less than 1% between the estimated first mode of the circular plate alone using the analytic approach, and that evaluated using numerical modal analysis.

The element size in the acoustic domain was chosen to follow the rule that there should be at least six elements per wavelength at the maximum frequency of the incident wave. The maximum frequency allowed in the analysis is limited by two factors:

1. In order to maintain plane wave propagation in the impedance tube the upper frequency limit should be defined as [55]:

$$f_u < \frac{c_o}{2d} \tag{33}$$

   Where $c_o$ is the speed of sound in the tube and $d$ is the largest dimension of the cross-section of the impedance tube.

2. The homogenization limit of the AMM cell which was chosen so that the wavelength of the incident wave was at least an order of magnitude larger than the largest dimension of the cell in the propagation direction i.e.:

$$f_u < \frac{c_o}{10a} \tag{34}$$

   Where $a$ is the width of the AMM cell.

For all the tested samples the upper frequency limit was mainly limited by the homogenization limit. For the dimensions of the cell in Table I, it was found to be around 1500 $Hz$.

For the 2D AMAM cell shown in Fig. 1b, the construction of the cell is the same for acoustic waves propagating in either x or y directions. This indicates that the material properties determined from one direction is sufficient to estimate the anisotropic material properties of the material. The cell has also half symmetry about the normal to the propagation direction, which suggests that the results obtained from the 1D AMAM cell could be used to characterize the 2D cell. To verify this assumption two different types of samples, shown in Fig. 3, were used in

to estimate the material properties. The first is a sample consisting of the full construction of the 2D cell (Fig. 1b). While the second was a simplified version consisting of only the 1D AMAM cell (Fig. 1d). For the 1D sample (Fig. 3a), since its cross section has a quarter symmetry, only a quarter sector of the tube and the cell was modeled. Symmetry boundary conditions were applied to the structural and acoustic domains. For the 1D AMAM, the number of cells forming the sample in the propagation direction were varied from 1 to 7 cells. This was done to check effect of varying the length of the material on the estimated material properties.

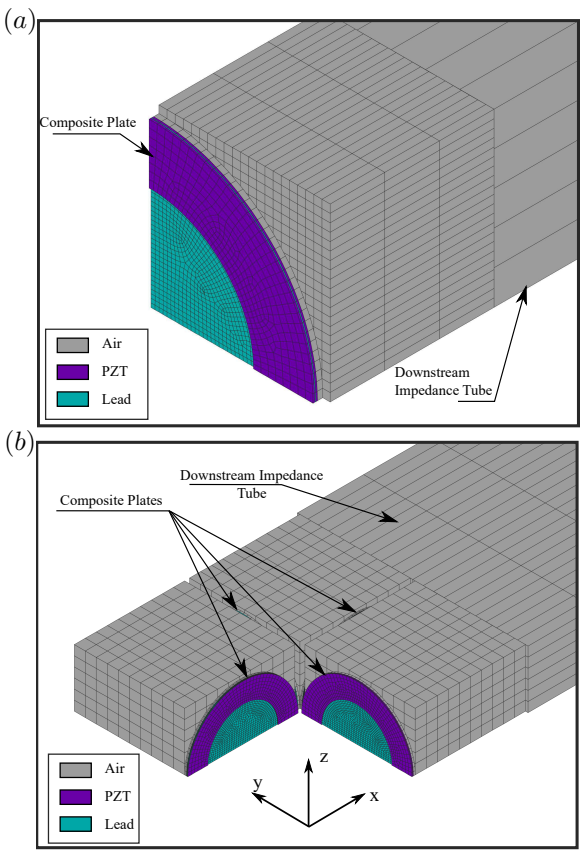


FIG. 3. A cross section in the finite element mesh of the (a) 1D AMAM sample with quarter symmetry placed in a square impedance tube, and (b) 2D AMAM sample with half symmetry placed in a rectangular impedance tube.

## IV. RESULTS AND DISCUSSION

The results obtained from the two types of FEM samples were found to be almost identical for the same number of cells in the direction of the incident excitation (Fig. 4 and Fig. 5). The same observation was noted for the results obtained from the analytic model whether using the 1D cell or by solving the acoustic network (Fig. 1c). Fig.4 and Fig. 6 also show that the calculated properties in the propagation direction (e.g. x) were independent from those of the direction normal to the propagation (e.g. y). The voltage applied to the cells normal to the x-direction was kept constant at zero voltage, and the voltage applied to those normal to the y-direction was varied from 0 to 300 $V$. No change in the properties estimated in the x-direction were observed. These two observations also confirm the assumption that the 1D AMAM cell shown in Fig.1d can be used to design and characterize the 2D material formed by repeating the same cell in two orthogonal directions. Fig. 4. shows the

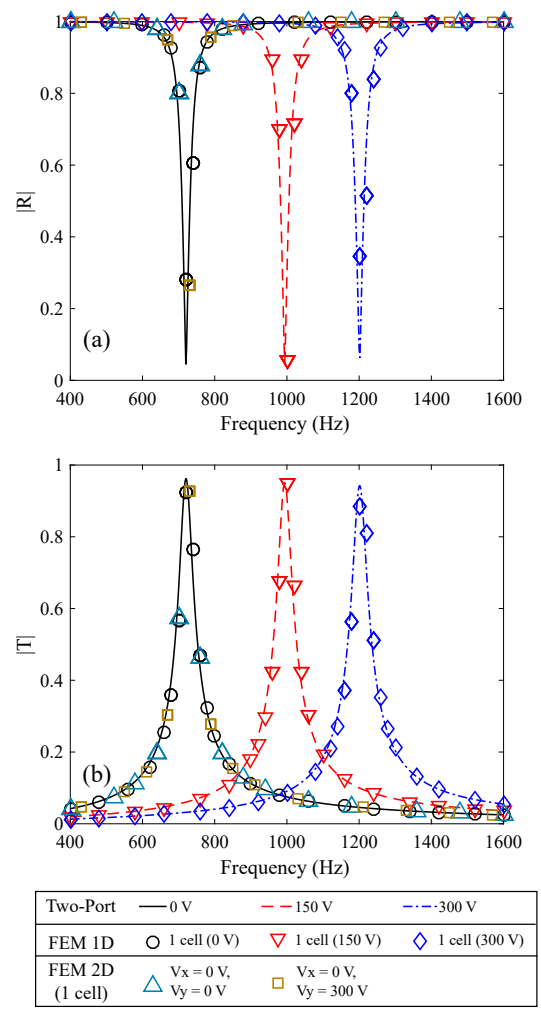


FIG. 4. The effect of applying different voltages on the amplitude of (a) $R$ and (b) $T$. The analytic two-port values are compared to those obtained from the FEM using one 1D AMAM cell in the incident wave propagation direction (x-direction), as well as, one 2D AMAM cell with the voltage being varied on the plates normal to the y-direction.

complex transmission and reflection coefficients obtained using the acoustic 2-Port model and the FEM. The results are evaluated for three different values of applied voltages. Good agreement is observed between the two methods for the range of the studied frequencies. Fig. 6a shows the Transmission Loss (TL) of a single 1D AMAM

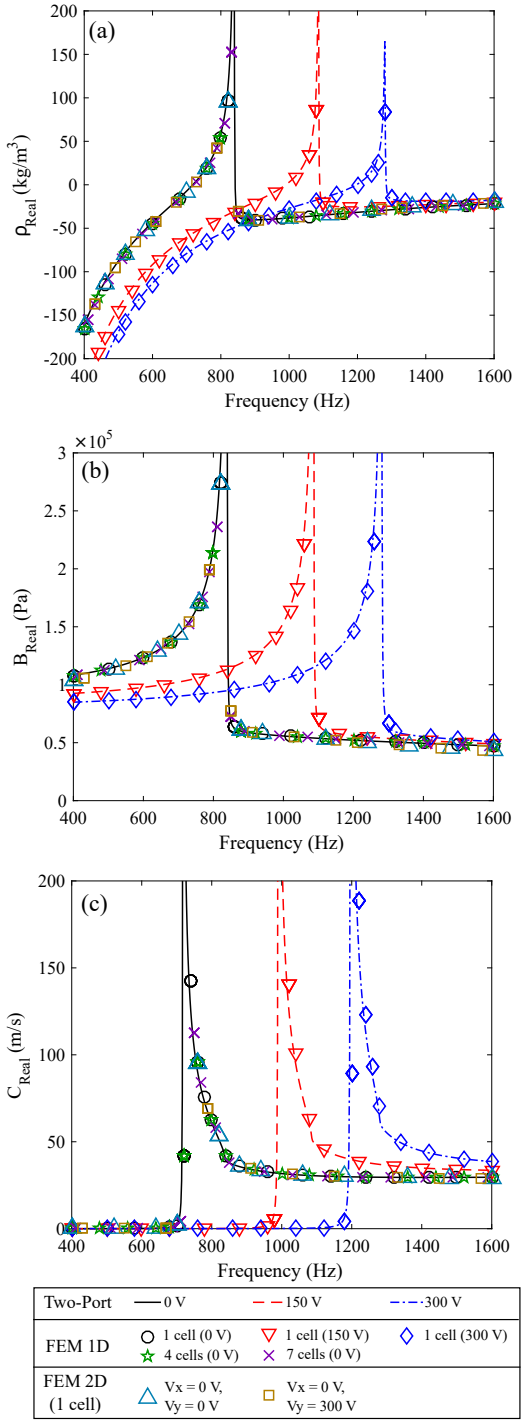


FIG. 5. The analytic and numerical dispersion plots for the real components of (a) the effective density, (b) effective bulk modulus and (c) the effective speed of sound estimated from (1, 4 and 7) 1D AMAM cells placed in the wave propagation direction (x-direction), as well as, one 2D AMAM cell while varying the voltage applied to the plates normal to the y-direction.

cell under three different applied voltages. The TL is defined as:

$$TL = 20log_{10}(\frac{1}{S_{21}}) \tag{35}$$

The trend of the transmission loss in Fig. 6a agrees with the general trend reported for the measured TL of a circular elastic plate clamped in a duct [52]. The effective ma-

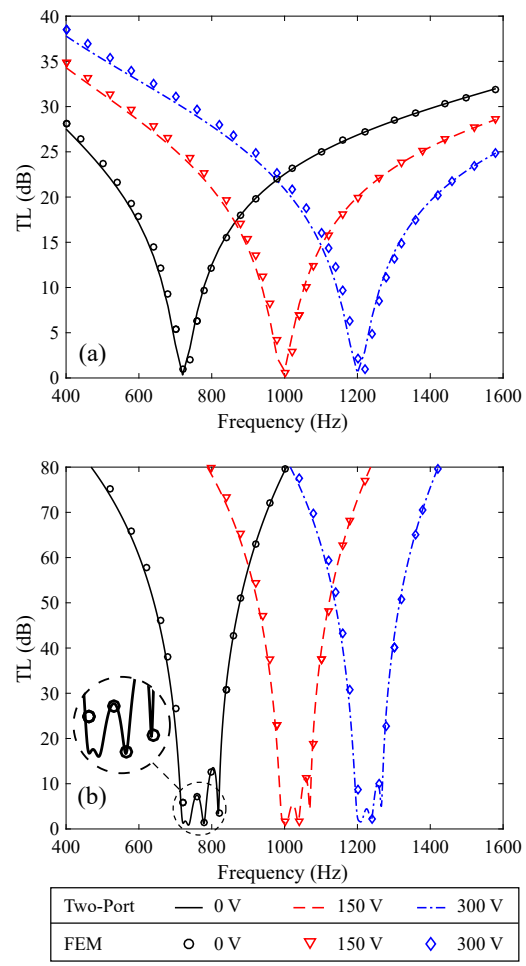


FIG. 6. The dispersion plot of the TL estimated from a sample consisting of (a) only one 1D AMAM cell and (b) four 1D AMAM cells in the propagation direction. The TL is calculated analytically (Lines) and using the FEM (Markers) with different voltages applied to the piezoelectric annulus $V = 0, 150, 300V$.

terial properties, mainly the effective density, bulk modulus and speed of sound, were calculated from the complex reflection and transmission coefficients. Their real components are shown in Fig. 5. The real component of the speed of sound (Fig. 5c), which represents the phase velocity of the sound waves inside the AMM, vanishes below the natural frequency of the composite plate. This indicates the presence of a stop band in this frequency region, which is similar to what was measured experimentally by

Lee et al.[2] for a membrane type AMM. They attributed the presence of the unusual stop band at this frequency region to the fact that the elastic restoring forces of the membrane below resonance cause a step reduction in the acoustic pressure across it. This leads to an exponential decay of the acoustic waves propagating through the material. From a material point of view, the effective density turns negative in this band (Fig. 5a), while the bulk modulus remains positive (Fig. 5b); as a result, the speed of sound becomes imaginary, since $c = \sqrt{\frac{B}{\rho}}$.
The effect of the applied voltage on the effective bulk modulus (Fig. 5b) for frequencies less than 700 Hz is small compared to its effect on the effective density (Fig. 5a). This enables us to control the density of the AMM with minimal effect on the bulk modulus in this region. This in turn facilitates using transformation acoustic techniques in the fabrication of acoustic devices, for example, the realization of acoustic cloaks. Fig. 5a shows that with no applied voltage, and for frequencies between $400 - 800Hz$, the effective density of the membrane increases from large negative values (about $-200\frac{kg}{m^3}$) passing by zero density at around $725Hz$ up to large positive values ($200\frac{kg}{m^3}$) with the increase of the frequency. By applying an electric voltage, we are able to shift the resonance of the composite plate, and thus the dispersion curve of the density. The magnitude of the shift is dependent on the magnitude of the applied voltage. If we consider controlling the effective density for a single frequency, Fig. 7 shows the dependency of the effective density on the applied voltage at different frequencies. It is clear that for the frequencies $(600, 720Hz)$, i.e. below the resonance of the composite plate under zero voltage, the relation between the applied voltage and the density is almost linear up to a voltage of $300V$. This means that a simple controller can be used to adjust the density of the cell at this frequency range. For higher frequencies, just below what is called the anti-resonance frequency of plate, the density of the plate is very sensitive to the applied voltage at low voltages, while it is less sensitive for higher voltages; nevertheless, it should be noted that with a suitable value of applied voltage the effective density at this frequency range can be controlled to vary between large positive and large negative values. A periodic arrangement of cells can only be considered as a material, if its effective material properties are invariant to its length. Thus in order to fulfill this condition, the effective material properties of different lengths of the suggested material should be compared to determine the frequency regions where the effective properties are invariant to the length. This can be done by the characterization of a sample consisting of more than a single cell in the propagation direction using the same homogenization technique. It should be noted that when calculating the effective material properties of multiple cells, the branch number $m$ in equation (7) and (8) plays an important role in calculating the correct properties. While for a single-cell sample $m$ can be safely assumed

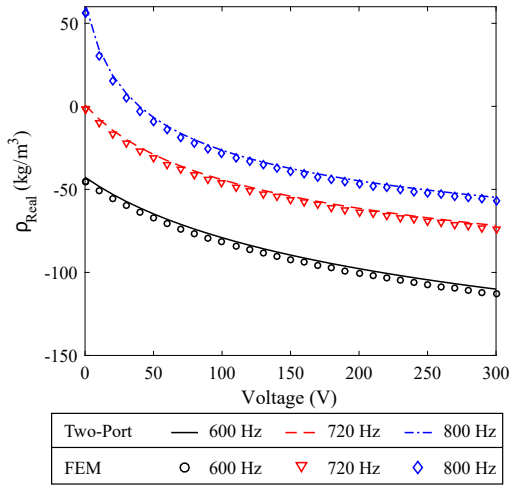


FIG. 7. The effect of the applied voltage on the real component of the effective density, which is calculated analytically (Lines) and using the FEM (Markers) for one 1D AMAM cell at three different frequencies namely $600, 720$ and $800Hz$.

to be zero (minimum thickness material), for multiple cells this is usually not the case and a proper method for selecting the branch number should be used.
The results for a sample consisting of four cells in the propagation direction is shown in Fig. 6b. Three new peaks appear in the dispersion plot of the transmission loss, that weren't observed in the single-cell sample (Fig. 6a). The calculated effective density, on the other hand, didn't show any variation if compared to the single-cell sample (Fig. 5a). The same observation was made for samples consisting of more cells than four, with a new peak appearing for each added cell and the same estimated effective properties (Fig. 5a). This confirms that the effective density (the material properties) of the studied cell is invariant to the length for the entire studied frequency range. This also further supports the claim that only one cell is sufficient to characterize the material using the retrieval method given in [46], given that the material is symmetric and the long wavelength region is maintained.

## V. APPLICATIONS

The structure of the 2D AMAM enables us to control its effective density in two different directions independently; moreover, the purposed structure can achieve near zero effective density. AMM with density-near-zero have been shown to possess extraordinary sound transmission characteristics [38, 57]. Combining the two advantages enables the developed material to be used in the fabrication of different acoustic devices which require controlling and manipulating the spatial propagation of acoustic waves. This includes reconfigurable waveguides, reconfigurable acoustic tunnels, tunable acoustic cloaks

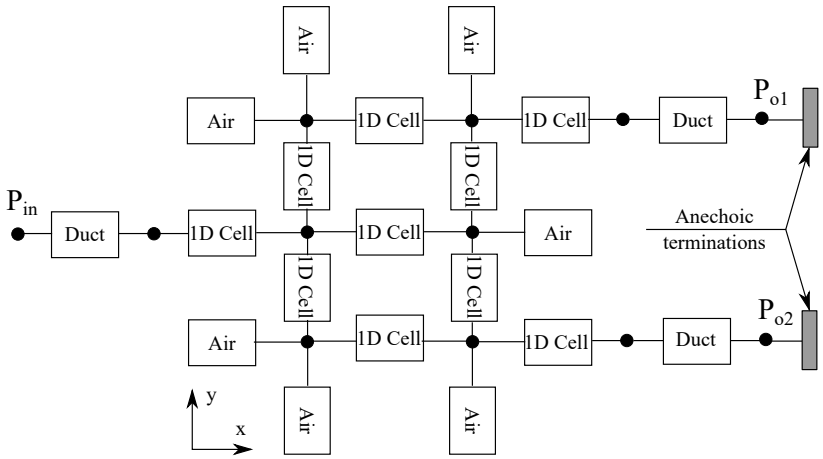


FIG. 8. The developed 2-port network model for the reconfigurable waveguide. The "Air" blocks indicates quarter cell sections terminated by the rigid walls of the guide. Incident pressure is applied to the node donated $P_{in}$.

and efficient noise control.

As a demonstration for the capabilities of the new designed cell, a simple controllable wave guide has been constructed. The guide consists of a $69 \times 46$ rectangular chamber filled with the new 2D AMAM and connected to three ducts. The ducts have $23 \times 23$ square cross sections and are fitted with anechoic terminations at the other ends.

Acoustic waves are incident to the guide from the left duct, and their direction of propagation is manipulated inside the chamber. By controlling the anisotropic effective density of each cell, the incident acoustic waves can be manipulated to exit the guide at any chosen location. This is done by setting the density of the required path for the wave inside the guide to near zero density, and at the same time setting the density of the other cells to large negative values which prevents the propagation of acoustic waves through them. The guide was modeled using the FEM by following a procedure similar to that mentioned in the 'Numerical Analysis' Section. An analytical model for the waveguide was also constructed using the network model for the 2D cell. The construction of the analytic network is shown in Fig. 8. Fig. 9a,9b shows the wave guide when all cells are set to density near zero, $\rho_{eff} = 0.2 kg/m^3$. This was done by applying $0\ V$ on all the cells for an incident wave of frequency $727\ Hz$. An efficient wave splitting is observed between the two output ducts. The configuration of the waveguide is changed in Fig.9c,d so that the wave propagation is limited to a path in which it is guided to exit from the upper duct. This was done by setting the density of the cells that are not on the desired path to $-70.15\ kg/m^3$ by applying $300\ V$ to them and leaving the cells on the path at near zero density. In the same manner the wave propagation could be controlled to exit from the lower duct. It is worth mentioning that by increasing the size of the wave guide, more ports and paths could be added to it. This would enable the usage of transformation acoustics techniques to create density fields that would allow for even more complex manipulations of the propagation of acoustic waves.

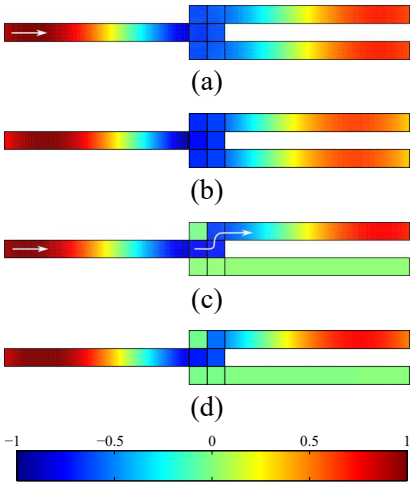


FIG. 9. The normalized pressure inside the suggested waveguide for an incident acoustic wave of frequency $727\ Hz$. The pressure is estimated using the FEM (a) and (c) and the analytic network model (b) and (d). The incident excitation and the propagation direction are marked with white arrows. The incident wave is controlled to (a),(b) split between the two ducts and (c),(d) exit from the upper duct only

## VI. CONCLUSION

We have introduced and analyzed a novel structure for active membrane-type acoustic metamaterials based on composite lead-PZT plates in air. The effective material properties of the metamaterial are estimated using the S-parameters retrieval method. An analytic model based on the acoustic two-port theory, the theory of piezoelectricity and the pre-stressed laminated plate

theory has been developed to analyze the material behavior. A FEM model was constructed to verify the analytic results using ANSYS.

The analytic results show good agreement with the FEM for all of the applied control voltages which opens the door to its use in the design of active acoustic metamaterials with similar construction, as well as in the implementation of controllers for the effective density of the material. The novel design has a frequency dependent effective density ranging from $-200\frac{kg}{m^3}$ to $200\frac{kg}{m^3}$ within a frequency range of $(400-1600Hz)$. We were able to analytically and numerically demonstrate that the effective density of the material can be controlled by applying a static voltage to the composite plate. The range of the controllable density lies within orders of magnitudes of the uncontrolled density while maintaining a minimum effect on the effective bulk modulus at frequencies below the resonance of the plate. This is achievable for the 2D cell where the anisotropic density could be controlled for two orthogonal directions independently from each other. The linear nature of the control characteristics of the material cell suggests that simple control techniques could be used to program each AMAM cell to a desired effective density. This facilitates the construction of devices consisting of large number of AMAM cells and hence the fabrication of devices which have full control on the directivity and dispersion characteristics of acoustic waves. The capabilities of the new design were demonstrated by the construction of fully reconfigurable wave guide in which the direction of propagation of incident acoustic waves could be arbitrarily programmed and controlled.


[1] H. H. Huang, C. T. Sun, and G. L. Huang. "On the negative effective mass density in acoustic metamaterials," *Int. J. Eng. Sci.*, **47**(4):610–617, April 2009.

[2] S. H. Lee, C. M. Park, Y. M. Seo, Z.G. Wang, and C.K. Kim. "Acoustic metamaterial with negative density," *Phys. Lett. A*, **373**(48):4464–4469, December 2009.

[3] N. Fang, D. Xi, J. Xu, M. Ambati, W. Srituravanich, C. Sun, and X. Zhang. "Ultrasonic metamaterials with negative modulus," *Nat Mater*, **5**(6):452–456, June 2006.

[4] S. H. Lee, C. M. Park, Y. M. Seo, Z. G. Wang, and C. K. Kim. "Acoustic metamaterial with negative modulus," *J. Phys.: Condens. Matter*, **21**(17):175704, April 2009.

[5] J. Li and C. Chan. "Double-negative acoustic metamaterial," *Phys. Rev. E*, **70**(5), November 2004.

[6] Y. Cheng, J. Xu, and X. Liu. "One-dimensional structured ultrasonic metamaterials with simultaneously negative dynamic density and modulus," *Phys. Rev. B*, **77**(4):045134, January 2008.

[7] D. Torrent and J. Snchez-Dehesa. "Anisotropic mass density by two-dimensional acoustic metamaterials," *New J. Phys.*, **10**(2):023004, February 2008.

[8] D. Torrent and J. Snchez-Dehesa. "Anisotropic Mass Density by Radially Periodic Fluid Structures," *Phys. Rev. Lett.*, **105**(17):174301, October 2010.

[9] L. Zigoneanu, B. I. Popa, A. F. Starr, and S. A. Cummer. "Design and measurements of a broadband two-dimensional acoustic metamaterial with anisotropic effective mass density," *J. Appl. Phys.*, **109**(5):054906, March 2011.

[10] J. Li, L. Fok, X. Yin, G. Bartal, and X. Zhang. "Experimental demonstration of an acoustic magnifying hyperlens," *Nat Mater*, **8**(12):931–934, December 2009.

[11] S. A. Cummer and D. Schurig. "One path to acoustic cloaking," *New J. Phys.*, **9**(3):45, March 2007.

[12] S. A. Cummer, B. I. Popa, D. Schurig, D. Smith, J. Pendry, M. Rahm, and A. Starr. "Scattering Theory Derivation of a 3d Acoustic Cloaking Shell," *Phys. Rev. Lett.*, **100**(2), January 2008.

[13] D. Torrent and J. Snchez-Dehesa. "Acoustic cloaking in two dimensions: a feasible approach," *New J. Phys.*, **10**(6):063015, June 2008.

[14] M. Fink. "Acoustic metamaterials: Nearly perfect sound absorbers," *Nat Mater*, **13**(9):848–849, August 2014.

[15] D. Torrent and J. Snchez-Dehesa. "Acoustic metamaterials for new two-dimensional sonic devices," *New J. Phys.*, **9**(9):323, September 2007.

[16] Z. Liu, X. Zhang, Y. Mao, Y. Y. Zhu, Z. Yang, C. T. Chan, and P. Sheng. "Locally Resonant Sonic Materials," *Science*, **289**(5485):1734–1736, September 2000.

[17] C. J. Naify, C. M. Chang, G. McKnight, and S. Nutt. "Transmission loss and dynamic response of membrane-type locally resonant acoustic metamaterials," *J. Appl. Phys.*, **108**(11):114905, December 2010.

[18] C. J. Naify, C. M. Chang, G. McKnight, F. Scheulen, and S. Nutt. "Membrane-type metamaterials: Transmission loss of multi-celled arrays," *J. Appl. Phys.*,**109**(10):104902, May 2011.

[19] L. Fok and X. Zhang. "Negative acoustic index metamaterial," *Phys. Rev. B*, **83**(21):214304, June 2011.

[20] F. Bongard, H. Lissek, and J. Mosig. "Acoustic transmission line metamaterial with negative/zero/positive refractive index," *Phys. Rev. B*, **82**(9):094306, September 2010.

[21] Y. M. Seo, J. J. Park, S. H. Lee, C. M. Park, C. K Kim, and S. H. Lee. "Acoustic metamaterial exhibiting four different sign combinations of density and modulus," *J. Appl. Phys.*, **111**(2):023504–023504–5, January 2012.

[22] M. Oudich, X. Zhou, and M. Badreddine Assouar. "General analytical approach for sound transmission loss analysis through a thick metamaterial plate," *J. Appl. Phys.*, **116**(19):193509, November 2014.

[23] M. Badreddine Assouar, M. Senesi, M. Oudich, M. Ruzzene, and Z. Hou. "Broadband plate-type acoustic metamaterial for low-frequency sound attenuation," *Appl. Phys. Lett.*, **101**(17):173505, October 2012.

[24] Y. Li, T. Chen, X. Wang, Y. Xi, and Q. Liang. "Enlargement of locally resonant sonic band gap by using composite plate-type acoustic metamaterial," *Phys. Lett. A*, **379**(5):412–416, February 2015.

[25] L. Airoldi and M. Ruzzene. "Design of tunable acoustic metamaterials through periodic arrays of resonant shunted piezos," *New J. Phys.*, **13**(11):113010, 2011.

[26] Y. Y. Chen, G. L. Huang, and C. T. Sun. "Band gap control in an active elastic metamaterial with negative capacitance piezoelectric shunting," *J. Vib. Acoust.*, **136**(6):061008, 2014.

[27] M. A. Nouh, O. J. Aldraihem, and A. Baz. "Periodic metamaterial plates with smart tunable local resonators," *J. Intel. Mat. Sys. Str.*, **27**(13):1829–1845, August 2016.

[28] H. Zhang, J. Wen, Y. Xiao, G. Wang, and X. Wen. "Sound transmission loss of metamaterial thin plates with periodic subwavelength arrays of shunted piezoelectric patches," *J Sound Vib.*, **343**:104–120, May 2015.

[29] W. Zhou, Y. Wu, and L. Zuo. "Vibration and wave propagation attenuation for metamaterials by periodic piezoelectric arrays with high-order resonant circuit shunts," *Smart Mater. Struct.*, **24**(6):065021, June 2015.

[30] F. Casadei, T. Delpero, A. Bergamini, P. Ermanni, and . Ruzzene. "Piezoelectric resonator arrays for tunable acoustic waveguides and metamaterials," *J. Appl. Phys.*, **112**(6):064902, September 2012.

[31] B. J. Kwon, J. Y. Jung, D. Lee, K. C. Park, and I. K. Oh. "Tunable acoustic waveguide based on vibro-acoustic metamaterials with shunted piezoelectric unit cells," *Smart Mater. Struct.*, **24**(10):105018, October 2015.

[32] P. Celli and S. Gonella. "Tunable directivity in metamaterials with reconfigurable cell symmetry," *Appl. Phys. Lett.*, **106**(9):091905, March 2015.

[33] A. Baz. "The structure of an active acoustic metamaterial with tunable effective density," *New J. Phys.*, 11(12):123010, December 2009.

[34] W. Akl and A. Baz. "Multicell Active Acoustic Metamaterial With Programmable Effective Densities," *J. Dyn. Sys., Meas., Control*, **134**(6):061001–061001, September 2012.

[35] W. Akl and A. Baz. "Experimental characterization of active acoustic metamaterial cell with controllable dynamic density," *J. Appl. Phys.*, **112**(8):084912, October 2012.

[36] X. Chen, X. Xu, S. Ai, H. Chen, Y. Pei, and X. Zhou. "Active acoustic metamaterials with tunable effective mass density by gradient magnetic fields," *Appl. Phys. Lett.*, **105**(7):071913, August 2014.

[37] S. Xiao, G. Ma, Y. Li, Z. Yang, and P. Sheng. "Active control of membrane-type acoustic metamaterial by electric field," *Appl. Phys. Lett.*, **106**(9):091904, March 2015.

[38] Y. Gu, Y. Cheng, J. Wang, and X. Liu. "Controlling sound transmission with density-near-zero acoustic membrane network," *J. Appl. Phys.*, **118**(2):024505, July 2015.

[39] M. L. Munjal. *Acoustics of Ducts and Mufflers With Application to Exhaust and Ventilation System Design*, Wiley-Interscience, New York, May 1987, pp. 55-57.

[40] R. Zhu, G. L. Huang, and G. K. Hu. "Effective Dynamic Properties and Multi-Resonant Design of Acoustic Metamaterials," *J. Vib. Acoust.*, **134**(3):031006–031006, April 2012.

[41] P. Li, S. Yao, X. Zhou, G. Huang, and G. Hu. "Effective medium theory of thin-plate acoustic metamaterials," *J. Acoust. Soc. Am.*, **135**(4):1844–1852, April 2014.

[42] S. Nygrd. *Low frequency modelling of complex duct networks*, Tech, Licent. Thesis, KTH, Marcus Wallenb. Lab. Sound Vib., 1999.

[43] X. Chen, T. Grzegorczyk, B.I. Wu, J. Pacheco, and J. Kong. "Robust method to retrieve the constitutive effective parameters of metamaterials," *Phys. Rev. E*, **70**(1), July 2004.

[44] D. R. Smith, D. C. Vier, Th. Koschny, and C. M. Soukoulis. "Electromagnetic parameter retrieval from inhomogeneous metamaterials," *Phys. Rev. E*, **71**(3), March 2005.

[45] Z. Szabo, G. H. Park, R. Hedge, and E. P. Li. "A Unique Extraction of Metamaterial Parameters Based on Kramers-Kronig Relationship," *IEEE T. Microw. Theory*, **58**(10):2646–2653, October 2010.

[46] V. Fokin, M. Ambati, C. Sun, and X. Zhang. "Method for retrieving effective properties of locally resonant acoustic metamaterials," *Phys. Rev. B*, **76**(14):144302, October 2007.

[47] B. I. Popa and S. Cummer. "Design and characterization of broadband acoustic composite metamaterials," *Phys. Rev. B*, **80**(17):174303, November 2009.

[48] B. I. Popa, L. Zigoneanu, and S. Cummer. "Tunable active acoustic metamaterials," *Phys. Rev. B*, **88**(2):024303, July 2013.

[49] N. Cselyuszka, M. Seujski, and V. Crnojevi-Bengin. "Analysis of Acoustic Metamaterials - Acoustic Scattering Matrix and Extraction of Effective Parameters," In *Proceedings of Metamaterials*, pages 17–22. Metamorphose VI, 2012.

[50] V. Lucarini, J. J. Saarinen, K. E. Peiponen, and E. M. Vartianen. *Kramers-Kronig Relations in Optical Materials Research,* Number v. 110 in Springer series in optical sciences. Springer, Berlin ; New York, 2005, pp. 27, 28.

[51] R. Glav and M. Abom. "A general formalism for analyzing acoustic 2-port networks," *J Sound Vib.*, **202**(5):739–747, 1997.

[52] J. E. Young. "Transmission of Sound through Thin Elastic Plates," *J. Acoust. Soc. Am.*, **26**(4):485–492, July 1954.

[53] J. N. Reddy. *Mechanics of Laminated Composite Plates and Shells: Theory and Analysis, Second Edition.* CRC Press, Boca Raton, June 2004, pp. 356, 357.

[54] M. Abom. "Measurement of the scattering-matrix of acoustical two-ports," *Mech. Syst. Signal Pr.*, **5**(2):89–104, March 1991.

[55] ASTM E2611 - 09. Standard Test Method for Measurement of Normal Incidence Sound Transmission of Acoustical Materials Based on the Transfer Matrix Method," Technical report, ASTM International, 2009.

[56] ANSYS, Inc. *ANSYS Mechanical APDL Acoustic Analysis Guide.* ANSYS, Inc., November 2013.

[57] R. Fleury and A. Al. "Extraordinary Sound Transmission through Density-Near-Zero Ultranarrow Channels," *Phys. Rev. Lett.*, **111**(5):055501, July 2013.